RSC Advances

ROYAL SOCIETY OF CHEMISTRY

www.rsc.org/advances

Cobalt modified mesoporous graphitic carbon nitride with enhanced visible-light photocatalytic activity

Pengxiang Qiu, Huan Chen and Fang Jiang*

Key Laboratory of Jiangsu Province for Chemical Pollution Control and Resources Reuse,School of Environmental and Biological Engineering, Nanjing University of Science and Technology, Nanjing 210094, PR China

*Corresponding author. Tel: +86-25-84311819; Fax:+86-25-84315352.

E-mail: fjiang@njust.edu.cn (F. Jiang)

Abstract

Mesoporous graphitic carbon nitride (mpg-C_3N_4) was synthesized using silica nanoparticles as the hard template, and cobalt modified mpg-C_3N_4 (Co_3O_4/mpg-C_3N_4) was prepared via a facile impregnation method. UV-Vis spectra showed that the mpg-C_3N_4 exhibited obvious absorption in the visible light range. The XPS results proved that the cobalt species deposited on mpg-C_3N_4 samples was Co_3O_4. The photocatalytic activity of Co_3O_4/mpg-C_3N_4 was evaluated in the photocatalytic degradation of bisphenol A (BPA) in aqueous solutions under visible light irradiation (λ>420 nm). The photocatalytic degradation efficiency of BPA by the Co_3O_4/mpg-C_3N_4 was significantly higher than that of mpg-C_3N_4 and an optimum content of Co_3O_4 loaded in the mpg-C_3N_4 was 1.5 wt. %. Radical-trapping experiments certified that both hydroxyl radicals and superoxide radicals were the active species for the photocatalytic degradation of BPA. The total organic carbon (TOC) removal showed that BPA was mineralized by 1.5% Co_3O_4/mpg-C_3N_4 under the visible light irradiation. The recycling tests indicated that 1.5% Co_3O_4/mpg-C_3N_4 was quite stable and there was no obvious decrease in photocatalytic activity after 5 cycles.

Key words: Co_3O_4/mpg-C_3N_4 photocatalyst; Visible-light photocatalysis; Bisphenol A

1. Introduction

Clean and sustainable solar energy has been extensively explored in order to overcome the serious energy and environmental challenges.[1-3] Some photocatalysts

such as TiO_2 exhibit high photocatalytic activity under UV due to their wide band gap (3.2 eV).[4] However, commercially available TiO_2 showed inefficient photocatalytic activity under visible light irradiation accounting for 43% of the solar spectrum. To make better use of the solar energy, the visible light responsive photocatalysts attracted more and more attention among researchers.

As a novel π-conjugated semiconductor (band gap=2.7 eV), the graphitic carbon nitride (g-C_3N_4) performs a high thermal (stable in O_2 up to 550 ^oC) and chemical stability (insoluble in solution with pH from 0 to 14). Moreover, g-C_3N_4 is an excellent and sustainable metal-free photocatalyst. Wang et al.[5-7] first reported that g-C_3N_4 showed the ability of hydrogen generation from water under visible light irradiation. However, the application of g-C_3N_4 is limited by the low adsorption of solar light and high recombination of photogenerated electron-hole pairs. A lot of attention has been focused on improving its photocatalytic activity. It was reported that nonmetallic elements doped g-C_3N_4 show prominent increase in photocatalytic activity. The efficiency of hydrogen generation from water by sulfur doped carbon nitride (g-CNS) was 12 times higher than that of g-C_3N_4.[8] Introducing boron into structural framework of g-C_3N_4 narrowed band gap of g-C_3N_4 to absorb more visible light.[9] The electric conductivity of P doped g-C_3N_4 is 4 orders of magnitude as much as g-C_3N_4.[10] F-doped g-C_3N_4 presented superior performances in the oxidization of benzene to phenol under visible light irradiation.[11] Meanwhile loading the noble metals (such as Ag,[12] Au,[13] Pd,[14] Pt[15]) can retard the recombination of electron-hole pairs to enhance the photocatalytic activity of the catalysts. Besides, integrating

g-C_3N_4 with other semiconductors could improve the light response. The photocatalytic degradation efficiency of 4-aminobenzoic acid by g-C_3N_4/CdS was 41.6 and 2.7 times higher than those of g-C_3N_4 and CdS.[16] Because of the enhancement of electron-hole separation on the interface of the semiconductors, the degradation efficiency of rhodamine B by $DyVO_4$/g-C_3N_4 was increased.[17] In addition, NiS/g-C_3N_4,[18] TiO_2/g-C_3N_4,[19] BiOI/g-C_3N_4,[20] BiOBr/g-C_3N_4,[21-22] ZnO/g-C_3N_4,[23] Bi_2WO_6/g-C_3N_4[24] and $ZnWO_4$/g-C_3N_4[25] composites also showed higher phtotcatalytic activities than individual g-C_3N_4. As all known, the large surface area of catalyst can afford more active sites for photocalysis. On the basis of this, the mesoporous graphitic carbon nitride (mpg-C_3N_4) which was synthesized using SiO_2 nanoparticles as hard template performed higher photocatalytic activity than g-C_3N_4.[26]

As a typical p-type nano-structured semiconductor, Co_3O_4 has attracted considerable attention in recent years due to its potential applications in batteries,[27] supercapacitors,[28] electrocatalysis,[29] and sensing devices.[30] Co_3O_4-based catalyst was synthesized for photocatalysis. Phenol was degraded efficiently over Co_3O_4/$BiVO_4$ composite under visible light irradiation.[31] Binitha et al.[32] prepared Co_3O_4 nanoflakes for photodegradation of dyes. Xiao et al.[33] researched photodegradation of methylene blue by Co_3O_4/$BiWO_6$ under visible light and found that the composite with 0.2 wt. % Co_3O_4 doping performed the highest photocatalytic activity. Pan et al.[34] prepared CuO/Co_3O_4 and investigated the mechanism of photocatalytic degradation of methyl orange on CuO/Co_3O_4 composite. Wang et al.[6] synthesized Co_3O_4 deposited g-C_3N_4 and investigated the photocatalytic oxidation of water by Co_3O_4/g-C_3N_4. But the

photocatalytic oxidation by Co_3O_4 loaded mpg-C_3N_4 has not been researched yet.

In this study, bulk g-C_3N_4, mpg-C_3N_4 and Co_3O_4/mpg-C_3N_4 with different loading of Co_3O_4 were prepared and their photocatalytic activities of BPA under visible light irradiation were investigated. The effect of Co_3O_4 in the photocatalytic reaction was researched and the photocatalytic mechanism was discussed.

2. Experimental

2.1. Preparation of bulk g-C_3N_4 and mpg-C_3N_4

All chemicals were of analytical grade and used without further purification. The bulk g-C_3N_4 was prepared by heating directly in ceramic crucible. Briefly, 5 g cyanamide was calcined for 4 h at 550 ^oC after heated at a rate of 2.3 ^oC min^{-1} to 550 ^oC. The mpg-C_3N_4 was prepared as reported with a few diversifications.[35] 10 g cyanamide solution (50 wt. %) was dissolved in 20 g solution with 40 wt. % of 12 nm SiO_2 particles (Ludox HS40, Aldrich) used as hard template. The mixture was stirred for 2 h at 80 ^oC. The resulting powder was calcined at 550 ^oC with a rate of 2.3 ^oC min^{-1} for 4 h in the air. Then yellow product was stirred in 4 mol L^{-1} NH_4HF for 24 h to remove the silica template. At last, the product was centrifuged and washed with distilled water and ethanol, and dried at 70 ^oC overnight.

2.2 Preparation of Co_3O_4 loaded mesoporous graphitic carbon nitride (Co_3O_4/mpg-C_3N_4)

The Co_3O_4/mpg-C_3N_4 catalysts with different Co_3O_4 loaded amounts were prepared by the conventional impregnation method. 1 g mpg-C_3N_4 was impregnated in $Co(NO_3)_2$ solution with different concentrations and evaporated under stirring at 90

^{o}C. The products were dried overnight and calcined at 300 ^{o}C for 2 h in the air. The products were donated as x % Co_3O_4/mpg-C_3N_4 where x standed for the mass of Co_3O_4/mpg-C_3N_4 mass percent.

2.3 Characterization of catalysts

X-ray diffraction (XRD) patterns were obtained in a Rigaku D/max-RA powder diffraction-meter using Cu Kα radiation. FT-IR spectra were obtained by a Nexus 870 FT-IR (Nicolet, USA) with KBr pellets. The transmission electron microscopy (TEM) images were obtained by JEOL 2100. The BET surface area analysis of the catalysts was accomplished at Micromeritics ASAP 2020. X-ray photoelectron spectroscopy (XPS) was recorded by a PHI 5000 VersaProbe. Photoluminescence spectra were carried out on a jobinYvon SPEX Fluorolog-3-P spectroscope. UV-vis diffuse reflectance spectroscopy (UV-vis-DRS) was performed with a Hitachi U-3010 UV-vis spectrometer. Photocurrent was obtained using a CHI 660B electrochemical workstation in a standard three-electrode system which used the products as the working electrodes. A 500 W xenon lamp worked as source of visible light irradiation.

2.4 Photocatalysis experiments

The photodegradation of BPA by catalysts was performed in a XPA-7 photochemical reactor (Xujiang Electromechanical plant Nanjing, China) and irradiated by a 500 W Xenon lamp. Briefly, 0.08 g catalyst was dispersed in 200 mL of 15 mg L^{-1} BPA solution in the quart tube reactor which was cooled by a thermostat. In order to reach adsorption-desorption equilibrium, the mixture was reacted in the

dark for 60 min before photocatalytic reaction. 2 mL suspension was gained at certain time intervals. After BPA samples were centrifuged and filtered, the concentration of BPA was measured by High Performance Liquid Chromatography (Ultimate 3000, Dionex) equipped with a Dionex Accliam@120 C18 column (4.6 nm * 250 nm) and emission wavelength of Fluorescence Detector was at 230 nm. The mobile-phase was 85% methanol and 15% water with a flow rate of 1 mL min^{-1} and the column temperature was set at 30 ℃.

3. Results and discussion

3.1 Catalyst characterization

Fig. 1a showed the XRD patterns of bulk g-C_3N_4 and Co_3O_4/mpg-C_3N_4 with different contents of Co_3O_4. For bulk g-C_3N_4, the strong peak at 27.4^o indexed as (002) was a characteristic interplanar stacking peak of the conjugated aromatic systems with the interlayer distance of 0.326 nm. In addition, a pronounced peak at 13.1^o corresponded to an in-plane structural packing motif, which was indexed as (100). The distance was determined to be 0.675 nm.[26, 33] For mpg-C_3N_4 and Co_3O_4/mpg-C_3N_4, the overall intensities of (002) and (100) peaks weakened and the intra layer periodicity corresponding to 13.1^o was broadened, which reflected the effect of geometric confinement. The previous studies reported that metal ion species restrained the polymeric condensation. The small amounts of the Co_3O_4 and good dispersion in the surface of Co_3O_4/mpg-C_3N_4 catalysts made no diffraction peaks of Co_3O_4 species observed in 1% Co_3O_4/mpg-C_3N_4, 1.5% Co_3O_4/mpg-C_3N_4, 2% Co_3O_4/mpg-C_3N_4 and 3% Co_3O_4/mpg-C_3N_4. For 5% Co_3O_4/mpg-C_3N_4, the diffraction

peaks at 30.8° and 44.1° were distributed to the (220) and (400) planes of Co_3O_4.[36-37]

Fig. 1b presented FT-IR spectra of 1.5 % Co_3O_4/mpg-C_3N_4 between 400 and 4000 cm^{-1}. The features of the condensed C−N heterocycles were also found on the spectra of Co_3O_4/mpg-C_3N_4. The typical triazine ring mode was at 808 cm^{-1} and its stretching mode was in the 1200-1650 cm^{-1} regions. The peaks observed at 1575 and 1634 cm^{-1} represented C=N stretching, while the three bands at 1245, 1321 and 1411 cm^{-1} were typical for the stretching vibrations of aromatic C-N. A broad adsorption band at 3157 cm^{-1} could be attributed to the stretching modes of terminal NH_2 or NH groups at the defect sites of the aromatic ring. Notably, an absorbance at 570 cm^{-1} was accompanied with the cobalt incorporation on the spectra of Co_3O_4/mpg-C_3N_4, which was ascribed to the combination bands of Co-O fundamental vibrational modes. It was revealed that the original graphitic C−N network did not alter after the inclusion of Co, which was in good agreement with the results of XRD analyses.

The TEM images of g-C_3N_4, mpg-C_3N_4 and 1.5% Co_3O_4/mpg-C_3N_4 were observed in Fig. 2. As shown in Fig. 2a, the bulk g-C_3N_4 exerted interlayer-like structure. And in Fig. 2b, the holes of mpg-C_3N_4 copied the hard template of Ludox HS40 entirely. The dark spherical spots corresponding to well-distributed Co_3O_4 nanoparticles in the surface of mpg-C_3N_4 were observed in Fig. 2c. Moreover, the import of the Co_3O_4 nanoparticles had little influence on the morphology of the catalysts.

N_2 adsorption/desorption isotherms were observed in Fig. 3a. For mpg-C_3N_4 and Co_3O_4/mpg-C_3N_4, the physioadsorption isotherms could be classified as type IV in the

IUPAC classification with a distinct hysteresis loop observed in the range of 0.5-1.0 P/P_0, which was characteristic of porous mater.[38] The BET specific surface of mpg-C_3N_4 was about 160.01 m^2 g^{-1}, which was slightly larger than that of Co_3O_4/mpg-C_3N_4 (149.62 m^2 g^{-1}). The pore size distribution was shown in Fig. 3b. The pores in catalysts were mainly distributed in the range 2-20 nm. The average pore size was about 12 nm attributed to the hard template of Ludox HS40. The introduction of Co_3O_4 slightly changed the BET specific surface and the mesoporous structure.

The XPS indicated the core level chemical shifts and characterize the bonding nature of 1.5 % Co_3O_4/mpg-C_3N_4. As shown in Fig. 4b, the peak at 284.6 eV corresponded to C-C coordination. The peak at 288.1 eV corresponding to the sp^2-hybridized carbon in N=C-N_2 was confirmed as originating from carbon atoms that have one double and two single bonds with three neighboring N atoms. The peak at a binding energy of 293.9 eV might be ascribed to π-excitation.[39-40] The XPS of N1s separating into four binding energies was observed in Fig. 4c. The primary peak at 398.6 eV was attributed to electrons originated from sp_2-hybridized N atoms in N=C-N_2.[5] The peak at 399.8 eV was ascribed to the tertiary nitrogen N-$(C)_3$ groups. The additional peak at 400.7 eV might be attributed to the amino functions carrying hydrogen (C-N-H), which corresponded to structural defects and incomplete condensation. The weak peak at 403.98 eV might be attributed to π-excitation.[39-40] The XPS of Co demonstrated a doublet corresponding to Co $2p_{3/2}$ and Co $2p_{1/2}$. Co $2p_{3/2}$ peak consisted of two peaks at 780.9 eV and 785.5 eV, which were ascribed to Co^{3+} and Co^{2+}. Co $2p_{1/2}$ similarly consisted of peaks at 797.1 eV and 802.9 eV, which

were attributed to Co^{3+} and Co^{2+}.[6, 31, 37] The relative contents of Co were calculated by the areas of the fitted Gaussian components in Fig. 4d with 70.24% Co^{3+} and 29.76% Co^{2+}. The result confirmed that Co in the form of the mixture (Co_3O_4) of Co^{3+} and Co^{2+} was loaded on the surface of mpg-C_3N_4.

3.2 Photodegradation of BPA

It was shown in Fig. 5a that the photodegradation of BPA by g-C_3N_4, mpg-C_3N_4 and 1.5 % Co_3O_4/mpg-C_3N_4. The results showed that BPA was hardly decomposed without catalysts under the visible light irradiation. The g-C_3N_4 represented very low photocatalytic activity and only 19.6% of BPA was degraded after irradiation for 180 min. Compared with g-C_3N_4, the photocatalytic efficiency of mpg-C_3N_4 was much higher, and 61.1% of BPA was degraded. Since the BET surface area of mpg-C_3N_4 was obviously larger than that of g-C_3N_4, mpg-C_3N_4 could furnish more catalytic active sites for reactions. The defects in the morphology of mpg-C_3N_4 improved the catalytic activity by the relocalization of electron in the graphitic layer. Furthermore, the appropriate pores were conducive to adsorption of the light waves deep inside the catalyst and the mobility of charges increased.[41-42] When 1.5% Co_3O_4 was presented on the surface of mpg-C_3N_4, the catalyst showed the highest photolytic efficiency that 93.6% of BPA was degraded under the visible light irradiation for 180 min. As a typical p-type semiconductor, Co_3O_4 could make great contributions to separate the electron-hole pairs. Thereby, the photocatalytic activity of mpg-C_3N_4 was enhanced by loading Co_3O_4.

The first-order kinetic model was used to describe the kinetic of the photodegradation of BPA:

$$C_t = C_0 \cdot e^{-k_{obs}t}$$

Where C_t is the concentration of BPA solution at reaction time t (min); C_0 is the initial concentration of BPA solution (mg L^{-1}); k_{obs} is the rate constant (min^{-1}). The experimental data fitted the first-order reaction kinetic model very well (R^2>0.99). The k_{obs} of the reactions with Co_3O_4/mpg-C_3N_4 containing different contents of Co_3O_4 were observed in Fig. 5b. The k_{obs} of 1.5% Co_3O_4/mpg-C_3N_4 (0.014 min^{-1}) was higher than that of 1% Co_3O_4/mpg-C_3N_4 (0.010 min^{-1}). It might be caused by the higher interfacial electron transfer efficiency which enhanced the photocatalytic activity with more loaded Co_3O_4. However, with the content of Co_3O_4 increasing to 5%, the k_{obs} decreased to 0.007 min^{-1}. Since the over abundance of metal behaved as recombination centers of electrons and holes which inhibited the separation of electrons-holes pairs. On the other hand, excess Co_3O_4 formed overlapping agglomerates and covered the active sites on the surface of catalyst. Therefore, 1.5% Co_3O_4/mpg-C_3N_4 exhibited the most outstanding activity.

It was reported that the initial pH of the solution affect the surface charge of the semiconductor catalysts and the ionization of the organic pollutants in aqueous solution. Fig. 5c revealed the photocatalytic efficiency of BPA in solution with different initial pH. As the initial pH increased from 3.01 to 12.89, the photocatalytic degradation efficiency decreased from 98.19% to 28.98%. Wang et al.[43] had reported that the nitrogen functionalities on the surface might act as strong Lewis base sites,

while the π-bonded planar layered configurations are expected to anchor phenol via special O-H···N or O-H···π interactions. Furthermore, O-H···N or O-H···π enhanced the adsorption of BPA on the surface of the catalyst. So the catalyst showed high BPA degradation efficiency at pH ranges from 3.01 to 10.05. The pK_a (acid dissociation constant) of BPA was reported as 9.6 to 11.3. When the value of pH was higher than pK_a of BPA, bisphenolate anion (-O-$C_{15}H_{14}$-O-) might be formed by (H-O-$C_{15}H_{14}$-O-H) due to deprotonation.[14,44-45] The interaction between BPA and the catalyst decreased which lead to less photodegradation efficiency at high pH>11.00.

3.3 Photocatalytic mechanism

The band structure of the photocatalyst is responsible for the efficient generation and separation process of the electron-hole pairs. The theoretical calculated values of the conduction band (CB) and valence band (VB) potentials of the mpg-C_3N_4 material were -1.13 and 1.57 eV, respectively.[31, 35] In the case of Co_3O_4, the values of the CB and VB potentials were 0.50 and 1.53 eV, respectively.[22] Based on the experimental and theoretical results, the reaction mechanism diagram of the Co_3O_4/mpg-C_3N_4 is presented in Fig. 6. With the induction of light, both Co_3O_4 and mpg-C_3N_4 can engender photogenerated electron-hole pairs. Because the VB of mpg-C_3N_4 is more positive than that of Co_3O_4, the holes mpg-C_3N_4 would migrate to the surface of Co_3O_4. Therefore, the electron-hole pairs can be efficiently separated on the composite interface and the charge recombination could be easily suppressed. As a result, the Co_3O_4/mpg-C_3N_4 catalyst possessed an enhanced photocatalytic activity.

The photoluminescence (PL) spectra of the photocatalysts indicated the

migration, transfer, and recombination processes of the photogenerated electron-hole pairs in the semiconductors.[46] Fig. 7a presented the PL spectra of g-C_3N_4, mpg-C_3N_4, and 1.5% Co_3O_4/mpg-C_3N_4 at the excitation wavelength of 400 nm. It could be seen that the emissions of g-C_3N_4, mpg-C_3N_4, and 1.5% Co_3O_4/mpg-C_3N_4 are centered at 460 nm, corresponding to the recombination process of self-trapped excitations. Compare to g-C_3N_4, the emission intensity of the mpg-C_3N_4 decreased remarkably, reflecting of the improved separation efficiency of electron-hole pairs. The emission intensity of the 1.5% Co_3O_4/mpg-C_3N_4 decreased further, suggesting that the presence of Co_3O_4 suppressed the recombination of the electron-hole pairs and consequently performed much higher photocatalytic activity.

The photocurrent measurements were carried out for mpg-C_3N_4 and Co_3O_4/mpg-C_3N_4 to investigate the synergistic effect between Co_3O_4 and mpg-C_3N_4. As observed in Fig. 7b, the photocurrent intensity of Co_3O_4/mpg-C_3N_4 (0.15 uA) was much higher than that generated by mpg-C_3N_4 (0.04 uA), demonstrating that the synergistic effect could improve markedly the separation efficiency of photoinduced electrons and holes.

The UV-vis diffuse reflectance spectra represented in Fig. 7c. The bulk g-C_3N_4 showed absorbance in a wide range of wavelength from UV to visible light and the wavelength of the absorption edge is 460 nm. Compared with the bulk g-C_3N_4, the absorption of light in mpg-C_3N_4 was enhanced. The pores were made for the deep adsorption of light waves on the catalyst as described previously. However, the light absorption of Co_3O_4/mpg-C_3N_4 increased markedly, which showed multiple bands at

550 nm and 760 nm that originated from $O^{2-} \rightarrow Co^{2+}$ and $O^{2-} \rightarrow Co^{3+}$ transitions.[47] Co_3O_4 enhanced the light absorption capacity of mpg-C_3N_4 in the range of near infrared and visible light, which made contributions to produce more electron-hole pairs. Therefore, the photocatalytic activity was enhanced by introducing Co_3O_4 nanoparticles on the surface of mpg-C_3N_4.

It was important to verify the main active oxidant in the photocatalytic reaction process. The active oxidants generated in the photocatalytic reaction were measured through trapped by t-BuOH (hydroxyl radicals scavenger), potassium iodide (photogenerated holes scavenger) and benzoquinone (superoxide radicals scavenger).[14] As shown in Fig. 8a, the photodegardation of BPA by the catalyst was restrained with the addition of t-BuOH. With presence of 1 mmol L^{-1} and 5 mmol L^{-1} t-BuOH, 89.5% and 80.4% of BPA were degraded. With the concentration of t-BuOH further increased to 10 mmol L^{-1}, the photocatalytic efficiency decreased slightly. It indicated that hydroxyl radicals played an important role in the photocatalytic degradation of BPA. Since the photodegardation of BPA was restrained with the addition of t-BuOH. However, the photocatalytic reaction of BPA was promoted with the presence of KI (Fig. 8b). It might be attributed to that scavenging h^+ improved the electron-hole separation and thus more free electrons generated more hydroxyl radicals.[48] Therefore, KI in the solution improved the photocatalytic efficiency. The photocatalysis was inhibited obviously with the degradation efficiency reduced to 34.9% as the concentration of benzoquinone was 1 mmol L^{-1}. With the concentration of benzoquinone up to 5 mmol L^{-1}, the suppression was not further intensified. It was

reported that the photogenerated electrons in the CB of graphitic carbon nitride could react with O^2 to generate $\bullet O_2^-$. Further, the superoxide radicals were momentous for the ring cleavage of aromatic compounds. Besides, the single-electron oxidation of phenoxyl radicals generated by phenols and the presence of $\bullet O_2$, phenoxyl radicals promoted the cleavage reactions of aromatic rings.[48-50] Hence, $\bullet O_2^-$ acted as major active radicals in the photocatalytic reaction. In conclusion, both hydroxyl radicals and superoxide radicals played important role in the photocatalytic reaction.

The TOC removal ratio was used to evaluate the mineralization efficiency of BPA by 1.5% Co_3O_4/mpg-C_3N_4 under visible light irradiation. As observed in Fig. 9, the TOC decreased gradually and the efficiency of TOC removal was 80.4%. It was noted that the efficiency of TOC removal was lower than that of photodegradation due to the incomplete mineralization of the BPA and generation of low molecular weight organic.

3.4 Stability of photocatalyst

Besides the activity of the photocatalyst, the stability is another significant effect on the assessment of the photocatalyst. Once the photocatalytic reaction of a testing cycle was completed, the suspension was filtered. The separated catalysts were washed with deionized water and dried at 70 ^oC before next testing cycle. As shown in Fig. 10, the cycles of the 1.5% Co_3O_4/mpg-C_3N_4 were performed to evaluate the stability of the photocatalyst. After 5 times cycles, the catalytic efficiency had slight decrease. Therefore, the 1.5% Co_3O_4/mpg-C_3N_4 showed significant stability, facilitating the application of the photocatalyst.

4. Conclusions

Co_3O_4 loaded mpg-C_3N_4 catalyst was prepared by the conventional impregnation method and the effects of contents of Co_3O_4 loaded on the photocatalytic activity were investigated. The highest degradation efficiency of BPA was achieved 93.6% by 1.5% Co_3O_4/mpg-C_3N_4. The catalyst showed high BPA degradation efficiency at pH ranges from 3.01 to 10.05. The benzoquinone and t-BuOH inhibited the photocatalytic reaction, while KI enhanced the reaction, indicating the hydroxyl radicals and the superoxide radicals were the major oxidative species in photocatalytic reaction. BPA was mineralized by Co_3O_4/mpg-C_3N_4 under the visible light irradiation. Besides the 1.5% Co_3O_4/mpg-C_3N_4 showed significant stability.

Acknowledgement

The financial supports from the Natural Science Foundation of China (No. 51178223 and 51208257), the Natural Science Foundation of Jiangsu Province (SBK201240759), China Postdoctoral Science Foundation (No. 2013M541677), the Jiangsu Planned Projects for Postdoctoral Research Funds and the project from Environmental Protection Department of Jiangsu Province of China (no. 2012008) are gratefully acknowledged.

References

1 D. Chatterjee and S. Dasgupta, *J. Photoch. Photobio.C.,* 2005, **6**, 186.

2 A. Fujishima and K. Honda, *Nature,* 1972, **238**, 37.

3 Y. Mu, H. Q. Yu, J. C. Zheng and S. J. Zhang, *J. Photoch. Photobio. A,* 2004, **163**,

311.

4 F. Jiang, S. Zheng, L. An, H. Chen, *Appl. Surf. Sci.,* 2012, **258**, 7188.

5 X. Wang, K. Maeda, A. Thomas, K. Takanabe, G. Xin, J. M. Carlsson, K. Domen and M. Antonietti, *Nat. Mater.,* 2008, **8**, 76.

6 J. Zhang, M. Grzelczak, Y. Hou, K. Maeda, K. Domen, X. Fu, M. Antonietti and X. Wang, *Chem. Sci.,* 2012, **3**, 443.

7 Y. Wang, X. Wang and M. Antonietti, *Angew. Chem. Int. Ed.,* 2012, **51**, 68.

8 J. Zhang, J. Sun, K. Maeda, K. Domen, P. Liu, M. Antonietti, X. Fu and X. Wang, *Energy . Environ. Sci.,* 2011, **4**, 675.

9 S. C. Yan, Z. S. Li and Z. G. Zou, *Langmuir,* 2010, **26**, 3894.

10 Y. Zhang and M. Antonietti, *J. Am. Chem. Soc.,* 2010, **132**, 6294.

11 Y. Wang, Y. Di, M. Antonietti, H. Li, X. Chen and X. Wang, *Chem. Mater.,* 2010, **22**, 5119.

12 Y. Meng, J. Shen, D. Chen and G. Xin, *Rare Metals,* 2011, **30**, 276.

13 N. Cheng, J. Tian, Q. Liu, C. Ge, A. H. Qusti, A. M. Asiri, A. O. Al-Youbi and X. Sun, *ACS Appl. Mater. Inter.,* 2013, **5**, 6815.

14 C. Chang, Y. Fu, M. Hu, C. Wang, G. Shan and L. Zhu, *Appl. Catal. B.,* 2013, **142-143**, 553.

15 K. Ghosh, M. Kumar, H. Wang, T. Maruyama and Y. Ando, *J. Phys. Chem. C.,* 2010, **114**, 5107.

16 J. Fu, B. Chang, Y. Tian, F. Xi and X. Dong, *J. Mater. Chem. A.,* 2013, **1**, 3083.

17 Y. He, J. Cai, T. Li, Y. Wu, Y. Yi, M. Luo and L. Zhao, *Ind. Eng. Chem. Res.,* 2012,

51, 14729.

18 J. Hong, Y. Wang, Y. Wang, W. Zhang and R. Xu, *ChemSusChem,* 2013, **6**, 2263.

19 X. Lu, Q. Wang and D. Cui, *J. Mater. Sci. Technol.,* 2010, **26**, 925.

20 C. Chang, L. Zhu, S. Wang, X. Chu and L. Yue, *ACS Appl. Mater. Inter.,* 2014, **6**, 5083.

21 J. Fu, Y. Tian, B. Chang, F. Xi and X. Dong, *J. Mater. Chem.,* 2012, **22**, 21159.

22 J. Di, J. Xia, S. Yin, H. Xu, M. He, H. Li, L. Xu and Y. Jiang, *RSC Adv.,* 2013, **3**, 19624.

23 J. X. Sun, Y. P. Yuan, L. G. Qiu, X. Jiang, A. J. Xie, Y. H. Shen and J. F. Zhu, *Dalton. T.,* 2012, **41,** 6756.

24 L. Ge, C. Han and J. Liu, *Appl. Catal. B.,* 2011, **108-109**, 100.

25 L. Sun, X. Zhao, C.J. Jia, Y. Zhou, X. Cheng, P. Li, L. Liu and W. Fan, *J. Mater. Chem.,* 2012, **22**, 23428.

26 F. Goettmann, A. Fischer, M. Antonietti and A. Thomas, *Angew. Chem. Int. Ed.,* 2006, **45**, 4467.

27 S. W. Hwang, A. Umar, S. H. Kim, S. A. Al-Sayari, M. Abaker, A. Al-Hajry and A. M. Stephan, *Electrochim. Acta.,* 2011, **56**, 8534.

28 X. Dong, H. Xu, X. Wang, Y. Huang, M. B. Chan-Park, H. Zhang, L. Wang, W. Huang and P. Chen, *ACS Nano*, 2012, **6**, 3206.

29 D. Zhang, Q. Xie, A. Chen, M. Wang, S. Li, X. Zhang, G. Han, A. Ying, J. Gong and Z. Tong, *Solid State Ionics,* 2010, **181**, 1462.

30 D. Barreca, D. Bekermann, E. Comini, A. Devi, R. A. Fischer, A. Gasparotto, M.

Gavagnin, C. Maccato, C. Sada, G. Sberveglieri and E. Tondello, *Sensor. Actuat. B.,* 2011, **160**, 79.

31 M. Long, W. Cai, J. Cai, B. Zhou, X. Chai and Y. Wu, *J. Phys. Chem. B.,* 2006, **110**, 20211.

32 N. N. Binitha, P. V. Suraja, Z. Yaakob, M. R. Resmi and P. P. Silija, *J. Sol-Gel. Sci. Techn.,* 2009, **53**, 466.

33 B. Jürgens, E. Irran, Jürgen. Senker, P. Kroll, H. Müller and W. Schnick, *J. Am. Chem. Soc.,* 2003, **125**, 10288.

34 L. Pan and Z. Zhang, *J. Mater. Sci-Mater. El.,* 2010, **21**, 1262.

35 A. Thomas, A. Fischer, F. Goettmann, M. Antonietti, J.O. Müller, R. Schlögl and J. M. Carlsson, *J. Mater. Chem.,* 2008, **18**, 4893.

36 Y. Q. Liang, Z. D. Cui, S. L. Zhu, Z. Y. Li, X. J. Yang, Y. J. Chen and J. M. Ma, *Nanoscale,* 2013, **5**, 10916.

37 Z. Ding, X. Chen, M. Antonietti and X. Wang, *ChemSusChem,* 2010, **4**, 274.

38 Y. Huang, Z. Ai, W. Ho, M. Chen and S. Lee, *J. Phys. Chem. C.,* 2010, **114**, 6342.

39 Y. Li, J. Zhang, Q. Wang, Y. Jin, D. Huang, Q. Cui and G. Zou, *J. Phys. Chem. B.,* 2010, **114**, 9429.

40 Q. Guo, Y.Xie, X. Wang, S. Zhang, T. Hou and S. Lv, *Chem. Commun.,* 2004, **1**，26.

41 X. Wang, J. Yu, C. Ho, Y. Hou and X. Fu, *Langmuir,* 2005, **21**, 2552.

42 L. Zhang and J. C. Yu, *Chem. Commun.,* 2003, **16**, 2078.

43 Y. Wang, J. Yao, H. Li, D. Su and M. Antonietti, *J. Am. Chem. Soc.,* 2011, **133**,

2362.

44 C. A. Staples, P. B. Dorn, G. M. Klecka, S. T. O'Block and L. R. Harris, *Chemosphere,*1998, **36**, 2149.

45 C. Wang, H. Zhang, F. Li and L. Zhu, *Environ. Sci. Technol.,* 2010, **44**, 6843.

46 J. Pal and P. Chauhan, *Mater. Charact.,* 2010, **61**, 575.

47 Y. Fu, H. Chen, X. Sun and X. Wang, *Appl. Catal. B.,* 2012, **111-112**, 280.

48 J. Ng, X. Wang and D. D. Sun, *Appl. Catal. B.,* 2011, **110**, 260.

49 P. Raja, A. Bozzi, H. Mansilla and J. Kiwi, *J. Photoch. Photobio. A.,* 2005, **169**, 271.

50 X. Wang, W. Yang, F. Li, Y. Xue, R. Liu and Y. Hao, *Ind. Eng. Chem. Res.,* 2013, **52**, 17140.

Figure captions:

Figure 1**.** (a) XRD patterns of g-C_3N_4, mpg-C_3N_4 and Co_3O_4/mpg-C_3N_4 with different contents of Co_3O_4 and (b) FT-IR spectra of 1.5% Co_3O_4/mpg-C_3N_4.

Figure 2. TEM images of (a) g-C_3N_4, (b) mpg-C_3N_4 and (c), (d) 1.5 % Co_3O_4/mpg-C_3N_4.

Figure 3. (a) N_2 adsorption-desorption isotherms and (b) pore size distributions of mpg-C_3N_4 and 1.5 %Co_3O_4/mpg-C_3N_4.

Figure 4. XPS spectra of 1.5 % Co_3O_4/mpg-C_3N_4: (a) full scan, (b) C 1s, (c) N 1s and (d) Co 2p.

Figure5. (a) Photocatalytic degradation of BPA under visible light irradiation in the presence of g-C_3N_4, mpg-C_3N_4, and 1.5 % Co_3O_4/mpg-C_3N_4; (b) The

pseudo-first-order rate constant (k_{obs}) for the photocatalytic degradation of BPA by Co_3O_4/mpg-C_3N_4 with different contents of Co_3O_4; (c) Influence of the initial pH on BPA degradation.

Figure 6. The schematic diagram of photocatalyticdegradation of BPA by 1.5% Co_3O_4/mpg-C_3N_4 catalyst under visible light irradiation.

Figure 7. (a) Photoluminescence spectra, (b) Photocurrent measurements, (c) UV-vis diffuse reflectance spectra of g-C_3N_4, mpg-C_3N_4 and 1.5% Co_3O_4/mpg-C_3N_4.

Figure 8. Photocatalytic degradation of BPA by 1.5% Co_3O_4/mpg-C_3N_4 with the addition of (a) t-BuOH, (b) KI and (c) benzoquinone.

Figure 9. Change in TOC abatements during photocatalytic degradation of BPA by 1.5% Co_3O_4/mpg-C_3N_4.

Figure 10. Cycling runs for the photocatalytic degradation of BPA in the presence of 1.5% Co_3O_4/mpg-C_3N_4.

Fig. 1

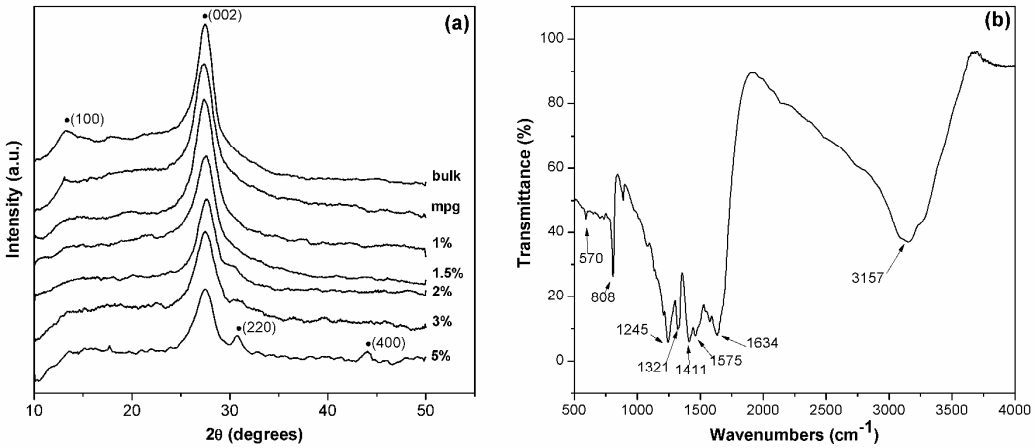

Fig. 2

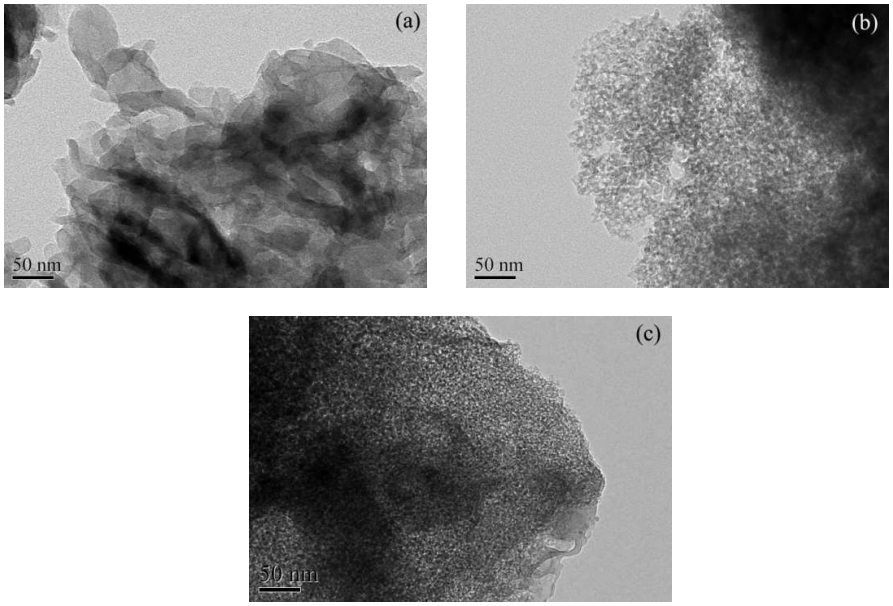

Fig. 3

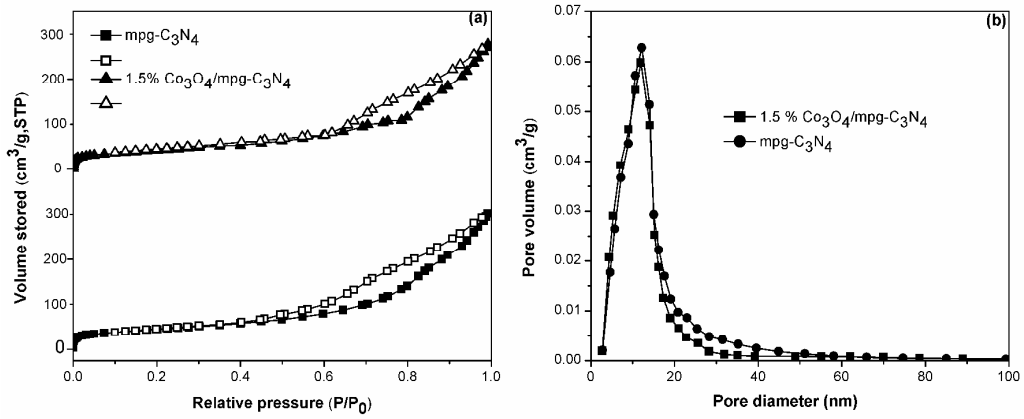

Fig. 4

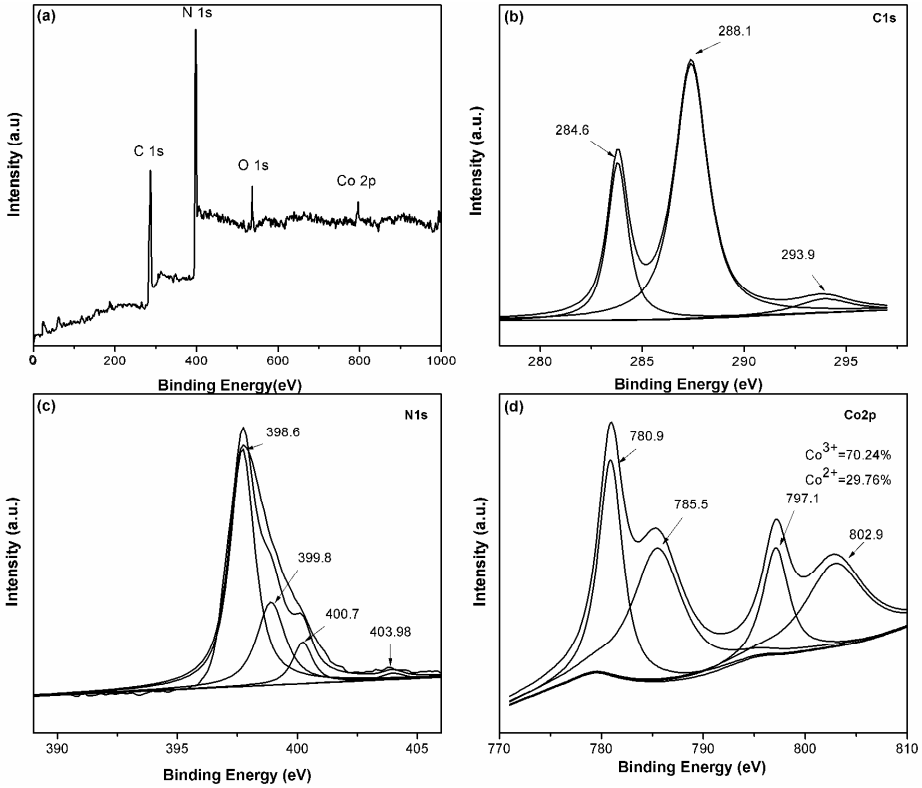

Fig. 5

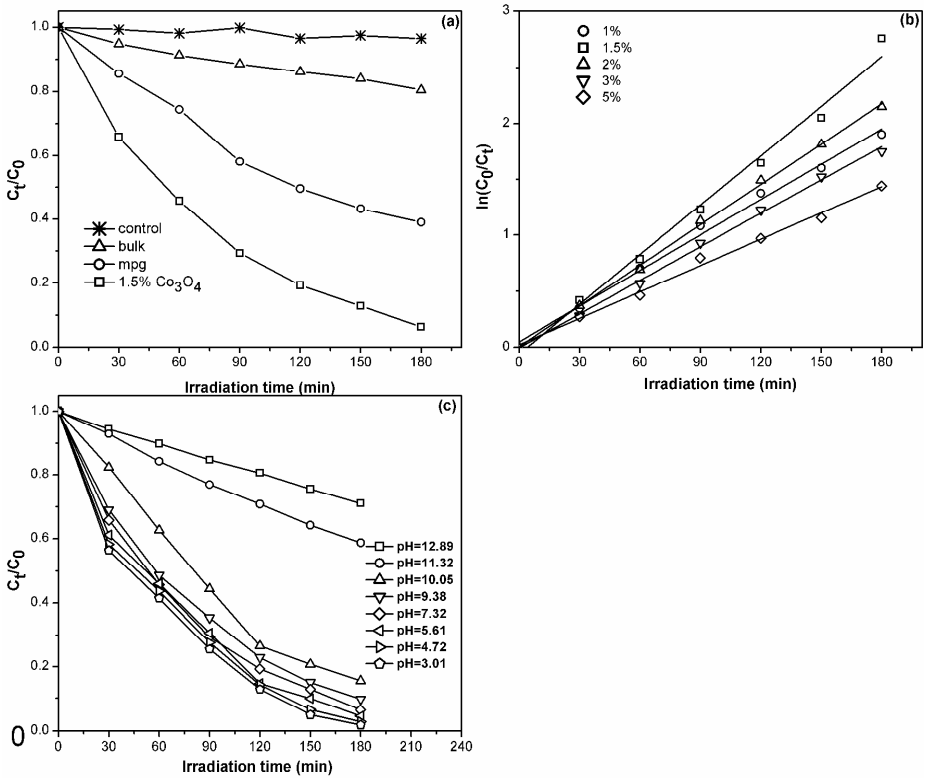

Fig.6

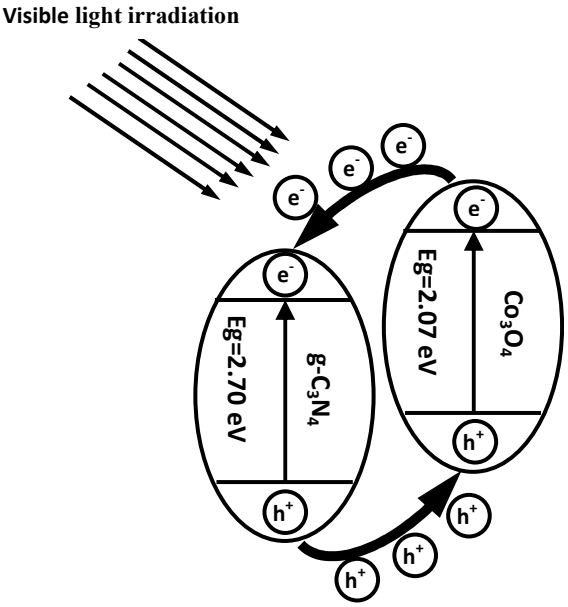

Fig.7

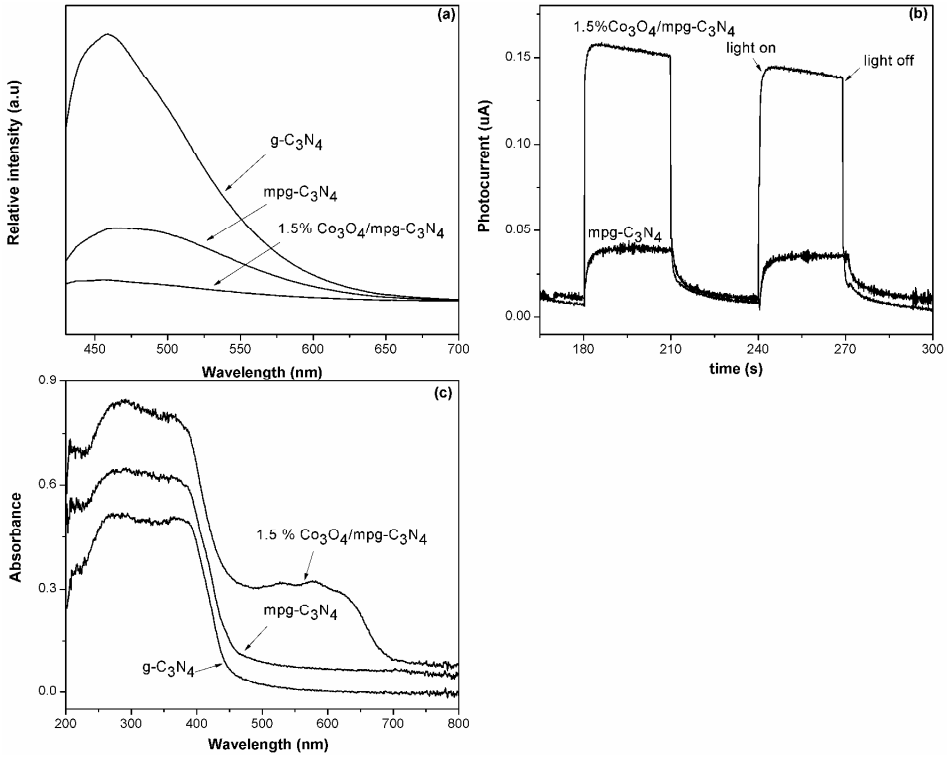

Fig.8

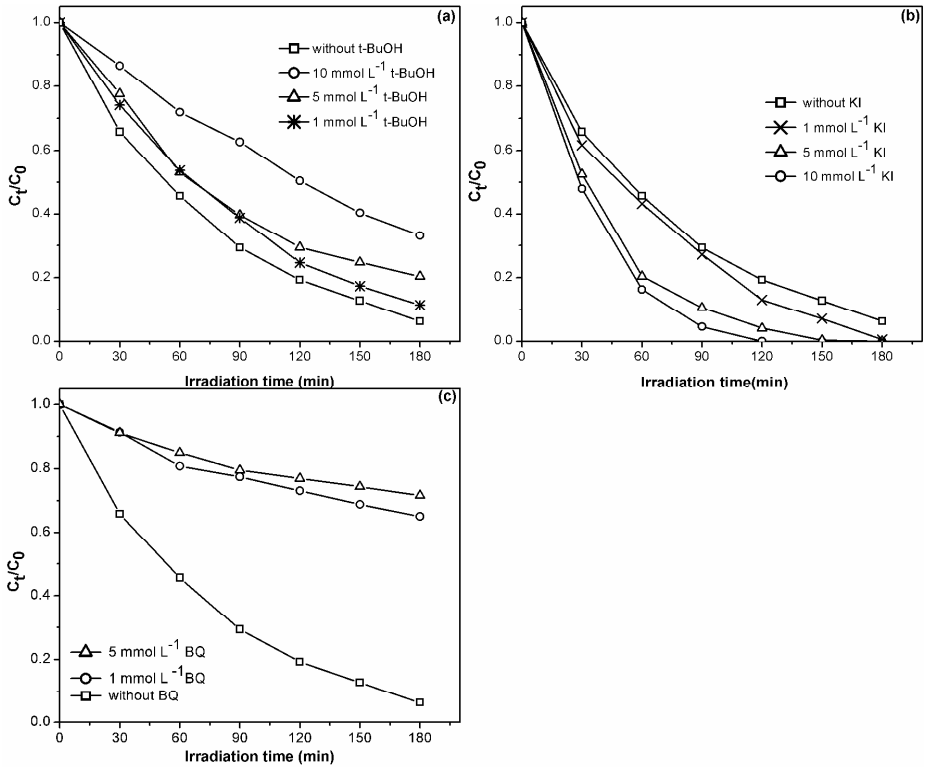

Fig. 9

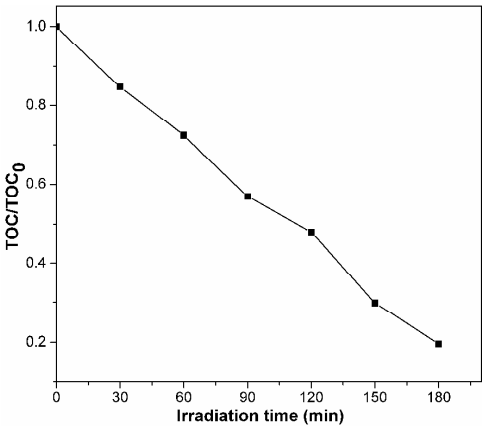

Fig. 10